Nonseparable Shearlet Transform

Wang-Q Lim

Abstract

Over the past years, various representation systems which sparsely approximate functions governed by anisotropic features such as edges in images have been proposed. Alongside the theoretical development of these systems, algorithmic realizations of the associated transforms were provided. However, one of the most common shortcomings of these frameworks is the lack of providing a unified treatment of the continuum and digital world, i.e., allowing a digital theory to be a natural digitization of the continuum theory. In this paper, we introduce a new shearlet transform associated with nonseparable shearlet generator which improves the directional selectivity of previous shearlet transforms. Our approach is based on discrete framework which allows a faithful digitization of the continuum domain directional transform based on compactly supported shearlets introduced as means to sparsely encode anisotropic singularities of multivariate data. We show numerical experiments demonstrating the potential of our new shearlet transform in 2D and 3D image processing applications.

Index Terms

Discrete shearlet transform, shearlets, wavelets, multiresolution analysis, sparse approximation.

EDICS Category: SMR-REP, TEC-MRS and TEC-RST

I. INTRODUCTION

One of the most important properties of wavelets is the connection between the wavelet transform in the continuum domain and filter banks in the digital domain. The connection was set up by a multiresolution analysis. Such a connection allows the wavelet transform, initially defined in the continuum domain, to be computed by a faithful digitization of the continuum theory, which provides a theoretical foundation for the discrete wavelet transform. However, multivariate functions are typically governed by anisotropic phenomena. For instance, edges in digital images are typically located along smooth curves owing to

This work was supported by DFG Grant SPP-1324, KU 1446/13-1. W. Lim is with Institute of Mathematics, TU Berlin, Berlin, Germany e-mail:lim@math.tu-berlin.de

smooth boundaries of physical objects. Although wavelets are good at isolating the discontinuities at edge points, the isotropic support of wavelets does not fit into efficiently capturing anisotropic features of edges. In addition, wavelets can detect only limited directional information. In order to overcome those major drawbacks of wavelets, several directional representation systems have been introduced (e.g. see [2],[5]). The main idea, in all of these constructions, is that, in order to obtain efficient representations of multi-variable functions with spatially distributed discontinuities, such representations must contain basis elements parametrized by scaling, translation and direction so that they provide many more shapes and directions than the classical wavelet bases. The main difficulty for digital implementation of such representations is how directional information can be identified in digital domain. Recall that, in the context of wavelet theory, faithful digitization is achieved by the concept of multiresolution analysis, where scaling and translation are digitized by discrete operations: downsampling, upsampling and convolution. In the case of directional transforms however, three types of operators: scaling, translation and direction, need to be digitized. None of digital directional transforms developed so far can provide fully faithful digitization of directional operator to the best of our knowledge. Shearlets have been introduced as means to sparsely encode piecewise smooth data and they are obtained by applying anisotropic scaling, shearing and translation to some fixed generating functions [7], [14]. In particular, unlike other directional representation schemes, directionality is obtained by shear matrix with integer entries and digital domain $\mathbb{Z}^2$ (and $\mathbb{Z}^3$) is invariant under this operator. In fact, this leads to faithfully digitized shearlet transform which allows a unified treatment of the continuum and digital world like the discrete wavelet transform. Such a discretization concept has been considered for the 2D shearlet transform with band-limited shearlets in [13] and with compactly supported shearlets generated by separable generating functions in [15]. This paper extends the work of [15] to establish a natural discretization of the continuum shearlet transform with compactly supported shearlets. Firstly, we will introduce a new way of discretizing shearlets originally defined in the continuum domain. Secondly, based on this, we will propose a new shearlet transform associated with compactly supported shearlets generated by nonseparable shearlet generators, which improves the directional selectivity of the shearlet transform based on separable shearlet generators.

This paper is organized as follows. In section II, we briefly review the definition of shearlets and the optimal sparse approximation properties of compactly supported shearlets. In section III, we discuss how to discretize the shear operator so that the directional information of digital data can be faithfully encoded. Based on this, we will derive a discrete shearlet transform using compactly supported shearlets in sections IV and V, In section VI, we will compare our algorithmic approach with other existing schemes. Then

we will show various applications of the shearlet transform in 2D and 3D image processing applications. Concluding remarks are drawn in section VIII.

II. SHEARLETS IN 2D AND 3D

In this section, we briefly overview the basic theory of shearlets in the continuum domain. Before this, let us start with a general mathematical notion of representation system, so called a frame. When designing representation systems of functions, it is sometimes beneficial to go beyond the setting of orthonormal bases and consider redundant systems. In particular, relaxing orthonormality of representation system can offer more flexibility of constructing system so that the elements of the system are well adapted for a signal f to provide sparse representation of f. Let us recall the basic definition of a frame in a Hilbert space $\mathcal{H}$.

Definition II.1. *A sequence $(\phi_i)_{i\in I}$ in a Hilbert space $\mathcal{H}$ is called a frame for H, if there exist constants $0 < A \leq B < \infty$ such that*

$$A\|f\|^2 \leq \sum_{i\in I} |\langle f, \phi_i\rangle|^2 \leq B\|f\|^2 \quad \textit{for all } f \in \mathcal{H}.$$

The notion of a frame guarantees stable reconstruction of a signal f decomposed into frame coefficients $\langle f, \phi_i\rangle$ as follows. The main operator associated with a frame is the frame operator

$$S : \mathcal{H} \to \mathcal{H}, \quad Sf = \sum_{i\in I} \langle f, \phi_i\rangle \phi_i.$$

In general, a signal $f \in \mathcal{H}$ can be recovered from its frame coefficients through the reconstruction formula

$$f = \sum_{i\in I} \langle f, \phi_i\rangle S^{-1}\phi_i. \tag{II.1}$$

The N–term approximation of a frame $(\phi_i)_{i\in I}$ is given by the index set I_N associated with the N largest frame coefficients $\langle f, \phi_i\rangle$ in magnitude as follows.

$$f_N = \sum_{i\in I_N} \langle f, \phi_i\rangle S^{-1}\phi_i.$$

With this generalized notion of representation system, we are now ready to define shearlet system for $L^2(\mathbb{R}^2)$.

Definition II.2. *For $j \geq 0$ and $k \in \mathbb{Z}$, define*

$$A_{2^j} = \begin{pmatrix} 2^j & 0 \\ 0 & 2^{\lfloor j/2\rfloor} \end{pmatrix} \quad \textit{and} \quad S_k = \begin{pmatrix} 1 & k \\ 0 & 1 \end{pmatrix}.$$

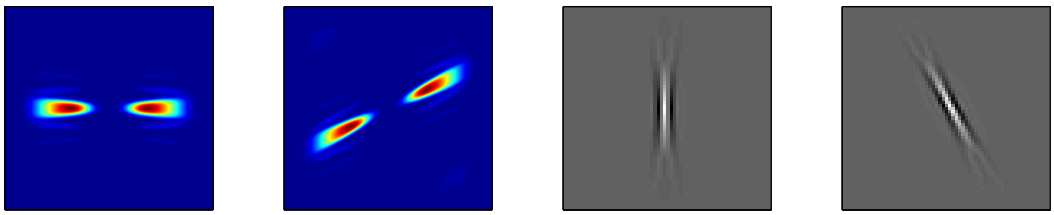

(a) (b) (c) (d)

Fig. 1. 2D shearlets $\psi_{j,k,m}$ in the spatial and frequency domain: (a) 2D plot of $|\hat{\psi}_{2,0,0}|$. (a) 2D plot of $|\hat{\psi}_{2,1,0}|$. (c) 2D plot of $\psi_{2,0,0}$ (d) 2D plot of $\psi_{2,1,0}$. Here, a nonseparable shearlet generator (IV.15) with the Symmlet wavelet 8-tap filter and 17×17 maximally flat 2D fan filter are used. A MATLAB routine *dfilters* from NSCT toolbox is used to compute the 2D fan filter.

Also, let $\tilde{A}_{2^j} = \text{diag}(2^j, 2^{\lfloor j/2 \rfloor})$. *For* $c = (c_1, c_2) \in (\mathbb{R}_+)^2$, *we now define*

$$\psi_{j,k,m} = 2^{(j+\lfloor j/2 \rfloor)/2} \psi(S_k A_{2^j} \cdot - \text{diag}(c_1, c_2)m)$$

and

$$\tilde{\psi}_{j,k,m} = 2^{(j+\lfloor j/2 \rfloor)/2} \tilde{\psi}(S_k^T \tilde{A}_{2^j} \cdot - \text{diag}(c_2, c_1)m).$$

Then, the (cone-adapted) regular discrete shearlet system *generated by a* scaling function $\phi \in L^2(\mathbb{R}^2)$ *and* shearlets $\psi, \tilde{\psi} \in L^2(\mathbb{R}^2)$ *is defined by*

$$\mathcal{SH}(c; \phi, \psi, \tilde{\psi}) = \Phi(c_1, \phi) \cup \Psi(c, \psi) \cup \tilde{\Psi}(c, \tilde{\psi}),$$

where

$$\Phi(c_1, \phi) = \{\phi_m = \phi(\cdot - c_1 m) : m \in \mathbb{Z}^2\},$$

$$\Psi(c, \psi) = \{\psi_{j,k,m} : j \geq 0, |k| \leq 2^{\lceil j/2 \rceil}, m \in \mathbb{Z}^2\}$$

and

$$\tilde{\Psi}(c, \tilde{\psi}) = \{\tilde{\psi}_{j,k,m} : j \geq 0, |k| \leq 2^{\lceil j/2 \rceil}, m \in \mathbb{Z}^2\}.$$

One key property of the shearlet system $\mathcal{SH}(c; \phi, \psi, \tilde{\psi})$ is that directionality is achieved by the shear matrix S_k which not only provides directionality but also leaves the integer grid $\mathbb{Z}^2$ invariant. In fact, this invariance property leads to a unified digitization concept for the shearlet transform between continuum and digital world as we will discuss in the next section. The following theorem shows sufficient conditions for the shearlet generators ψ and $\tilde{\psi}$ to generate a frame [10].

Theorem II.3. *Let $\phi, \psi \in L^2(\mathbb{R}^2)$ be such that*

$$\hat{\phi}(\xi_1, \xi_2) \leq C_1 \min\{1, |\xi_1|^{-\gamma}\} \min\{1, |\xi_2|^{-\gamma}\}$$

and

$$|\hat{\psi}(\xi_1, \xi_2)| \leq C_2 \min\{1, |\xi_1|^{\alpha}\} \min\{1, |\xi_1|^{-\gamma}\} \min\{1, |\xi_2|^{-\gamma}\}, \tag{II.2}$$

for some positive constants $C_1, C_2 < \infty$ and $\alpha > \gamma > 3$. Define $\tilde{\psi}(x_1, x_2) = \psi(x_2, x_1)$. We also assume that there exists a positive constant $A > 0$ such that

$$|\hat{\phi}(\xi)|^2 + \sum_{j \geq 0} \sum_{|k| \leq 2^{\lceil j/2 \rceil}} |\hat{\psi}(S_k^T A_{2^{-j}} \xi)|^2 + |\hat{\tilde{\psi}}(S_k \tilde{A}_{2^{-j}} \xi)|^2 > A \tag{II.3}$$

Then there exists a sampling parameter $c = (c_1, c_2) \in (\mathbb{R}^+)^2$ such that the shearlet system $\mathcal{SH}(c; \phi, \psi, \tilde{\psi})$ forms a frame for $L^2(\mathbb{R}^2)$.

Notice that there are many compactly supported function ψ satisfying the conditions (II.2). In particular, one can choose compactly supported wavelets as shearlet generators ψ. This choice will guarantee stable reconstruction (II.1) from the shearlet coefficients $\langle f, \psi_{j,k,m} \rangle$ provided that ψ is sufficiently smooth and has enough vanishing moments. Fig 2 shows frequency covering associated with shearlets which covers

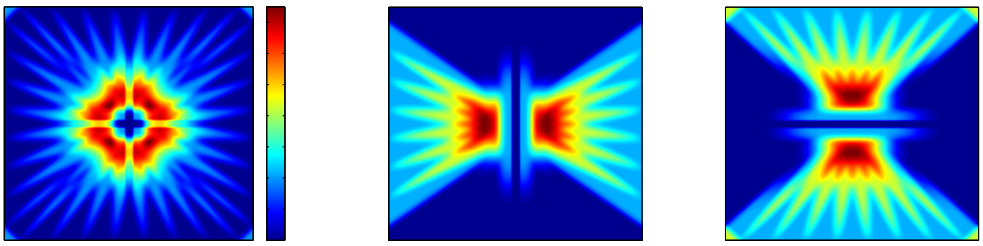

(a) (b) (c)

Fig. 2. Frequency covering by shearlets: (a) Frequency covering of the entire frequency plane. (b) Frequency covering by $|\hat{\psi}_{j,k,m}|^2$ for the horizontal cone. (c) Frequency covering by $|\hat{\tilde{\psi}}_{j,k,m}|^2$ for the vertical cone. Here, a separable shearlet generator with the Symmlet wavelet 8-tap filter is used.

2D frequency plane except for low frequency part. The low frequency part is covered by the scaling functions ϕ_m like the wavelet system. Taking all frequency supports of shearlets $\psi_{j,k,m}$ covers a region of the horizontal cones as illustrated in Fig. 2(b). In this case, the directional angles between $-\pi/4$ and $\pi/4$ are covered since the shear parameters satisfy $k \geq -2^{\lceil j/2 \rceil}$ and $k \leq 2^{\lceil j/2 \rceil}$. Similarly, a region of

the vertical cones is covered by supp($\hat{\tilde{\psi}}_{j,k,m}$) as illustrated in Fig. 2(c). Note that shear matrices S_k and $\tilde{S}_k^T$ behave similar to rotations for $|k| \leq 2^{\lceil j/2 \rceil}$ which gives directionality.

We now extend 2D shearlets to 3D case. 3D shearlets are scaled according to the *paraboloidal scaling matrices* A_{2^j}, $\tilde{A}_{2^j}$ or $\breve{A}_{2^j}$, $j \in \mathbb{Z}$ defined by

$$A_{2^j} = \text{diag}(2^j, 2^{\lfloor j/2 \rfloor}, 2^{\lfloor j/2 \rfloor}), \;\; \tilde{A}_{2^j} = \text{diag}(2^{\lfloor j/2 \rfloor}, 2^j, 2^{\lfloor j/2 \rfloor})$$

and

$$\breve{A}_{2^j} = \text{diag}(2^{\lfloor j/2 \rfloor}, 2^{\lfloor j/2 \rfloor}, 2^j)$$

and directionality is encoded by the *shear matrices* S_k, $\tilde{S}_k$, or $\breve{S}_k$, $k = (k_1, k_2) \in \mathbb{Z}^2$, given by

$$S_k = \begin{pmatrix} 1 & k_1 & k_2 \\ 0 & 1 & 0 \\ 0 & 0 & 1 \end{pmatrix}, \quad \tilde{S}_k = \begin{pmatrix} 1 & 0 & 0 \\ k_1 & 1 & k_2 \\ 0 & 0 & 1 \end{pmatrix}, \quad \text{and} \quad \breve{S}_k = \begin{pmatrix} 1 & 0 & 0 \\ 0 & 1 & 0 \\ k_1 & k_2 & 1 \end{pmatrix},$$

respectively. The translation lattices will be defined through the following matrices: $M_c = \text{diag}(c_1, c_2, c_2)$, $\tilde{M}_c = \text{diag}(c_2, c_1, c_2)$, and $\breve{M}_c = \text{diag}(c_2, c_2, c_1)$, where $c_1 > 0$ and $c_2 > 0$. From this, we define

$$\begin{aligned} \psi_{j,k,m} &= 2^{(j+2\lfloor j/2 \rfloor)/2} \psi(S_k A_{2^j} \cdot - M_c m) \\ \tilde{\psi}_{j,k,m} &= 2^{(j+2\lfloor j/2 \rfloor)/2} \tilde{\psi}(\tilde{S}_k \tilde{A}_{2^j} \cdot - \tilde{M}_c m) \end{aligned}$$

and

$$\breve{\psi}_{j,k,m} = 2^{(j+2\lfloor j/2 \rfloor)/2} \breve{\psi}(\breve{S}_k \breve{A}_{2^j} \cdot - \breve{M}_c m).$$

We are ready to introduce 3D shearlet systems, for which we will make use of the vector notation $|k| \leq K$ for $k = (k_1, k_2)$ and $K > 0$ to denote $|k_1| \leq K$ *and* $|k_2| \leq K$.

Definition II.4. *For $c = (c_1, c_2) \in (\mathbb{R}_+)^2$, the* pyramid-adapted discrete shearlet system $SH(\phi, \psi, \tilde{\psi}, \breve{\psi}; c)$ *generated by $\phi, \psi, \tilde{\psi}, \breve{\psi} \in L^2(\mathbb{R}^3)$ is defined by*

$$\mathcal{SH}(\phi, \psi, \tilde{\psi}, \breve{\psi}; c) = \Phi(\phi; c_1) \cup \Psi(\psi; c) \cup \tilde{\Psi}(\tilde{\psi}; c) \cup \breve{\Psi}(\breve{\psi}; c),$$

where

$$\begin{aligned}
\Phi(\phi; c_1) &= \left\{\phi(\cdot - m) : m \in c_1\mathbb{Z}^3\right\}, \\
\Psi(\psi; c) &= \left\{\psi_{j,k,m} : j \geq 0, |k| \leq 2^{\lceil j/2 \rceil}, m \in \mathbb{Z}^3\right\}, \\
\tilde{\Psi}(\tilde{\psi}; c) &= \{\tilde{\psi}_{j,k,m} : j \geq 0, |k| < 2^{\lceil j/2 \rceil}, m \in \mathbb{Z}^3\}, \\
\textit{and} \quad \breve{\Psi}(\breve{\psi}; c) &= \{\breve{\psi}_{j,k,m} : j \geq 0, |k| < 2^{\lceil j/2 \rceil}, m \in \mathbb{Z}^3\},
\end{aligned}$$

where $j \in \mathbb{N}_0$ *and* $k \in \mathbb{Z}^2$. *with* $\lambda = (j, k, m)$.

In this case, 3D frequency domain is partitioned into three pairs of pyramids and restricting the range of the shear parameters to $[-2^{\lceil j/2 \rceil}, 2^{\lceil j/2 \rceil}]$ makes shear matrices S_k, $\tilde{S}_k$ and $\breve{S}_k$ behave similar to rotations as in 2D case. Define $\tilde{\psi}(x) = \psi(x_2, x_1, x_3)$ and $\breve{\psi}(x) = \psi(x_3, x_2, x_1)$ for $x = (x_1, x_2, x_3) \in \mathbb{R}^3$ where

$$|\hat{\psi}(\xi)| \leq C_2 \cdot \min\{1, |\xi_1|^\delta\} \cdot \min\{1, (\xi_1^2 + \xi_2^2 + \xi_3^2)^{-\gamma/2}\} \tag{II.4}$$

for some constants $C_1, C_2 > 0$ and $\delta > 2\gamma > 6$. Then the 3D shearlet system $\mathcal{SH}(\phi, \psi, \tilde{\psi}, \breve{\psi}; c)$ forms a frame for $L^2(\mathbb{R}^3)$ provided that a 3D version of covering condition (II.3) is satisfied. We refer to [8] for more details. Finally, it can be shown that compactly supported shearlet systems provide nearly optimally sparse approximations for C^2 piecewise smooth functions f which are C^2 smooth apart from C^2 discontinuity curve or surface. This property holds for both 2D and 3D. We refer to [9] and [8] for more details. In particular, for such 2D piecewise smooth functions $f \in L^2(\mathbb{R}^2)$, we have

$$\|f - f_N\|_2^2 \leq C(\log(N))^3 N^{-2},$$

where f_N is the $N-$term shearlet approximation.

III. Faithful Discretization of Shear Operator

In this section, we will derive a fast algorithm which explicitly computes the shearlet coefficients $\langle f, \psi_{j,k,m} \rangle$. In particular, we will discuss how the shear operator S_k can be naturally adapted to the digital domain $\mathbb{Z}^2$. Let ψ^1 and $\phi^1 \in L^2(\mathbb{R})$ be a wavelet and an associated scaling function satisfying two scale equations

$$\phi^1(x_1) = \sum_{n1 \in \mathbb{Z}} h(n_1)\sqrt{2}\phi^1(2x_1 - n_1) \tag{III.5}$$

and

$$\psi^1(x_1) = \sum_{n1 \in \mathbb{Z}} g(n_1)\sqrt{2}\phi^1(2x_1 - n_1). \tag{III.6}$$

Then wavelets ψ^1_{j,n_1} are defined by

$$\psi^1_{j,n_1}(x_1) = 2^{j/2}\psi^1(2^j x_1 - n_1).$$

For $j > 0$, let $(h_j(n_1))_{n1\in\mathbb{Z}}$ and $(g_j(n_1))_{n1\in\mathbb{Z}}$ be the Fourier coefficients of trigonometric polynomials

$$\hat{h}_j(\xi_1) = \prod_{k=0}^{j-1} \hat{h}(2^k\xi_1) \quad \text{and} \quad \hat{g}_j(\xi_1) = \hat{g}(2^{j-1}\xi_1)\hat{h}_{j-1}(\xi_1),$$

where

$$\hat{h}(\xi_1) = \sum_{n_1\in\mathbb{Z}} h(n_1)e^{-2\pi i n_1\xi_1}, \hat{g}(\xi_1) = \sum_{n_1\in\mathbb{Z}} g(n_1)e^{-2\pi i n_1\xi_1}.$$

Suppose that

$$f^{1\mathrm{D}}(x_1) = \sum_{n_1\in\mathbb{Z}} f^{1\mathrm{D}}_J(n_1)2^{J/2}\phi_1(2^J x_1 - n_1).$$

Then the wavelet coefficients $\langle f^{1\mathrm{D}}, \psi^1_{j,n_1}\rangle$ are computed by the following discrete formula:

$$\langle f^{1\mathrm{D}}, \psi^1_{j,m_1}\rangle = \overline{w}_j * (f^{1\mathrm{D}}_J * \Phi^1)(2^{J-j}\cdot m_1), \tag{III.7}$$

where $w_j \equiv g_{J-j}$, $\overline{w}_j(n_1) = w_j(-n_1)$ and $\Phi^1(n_1) = \langle\phi^1(\cdot), \phi^1(\cdot - n_1)\rangle$. In particular, when ϕ_1 is an orthonormal scaling function we have

$$\langle f^{1\mathrm{D}}, \psi^1_{j,m_1}\rangle = \overline{w}_j * (f^{1\mathrm{D}}_J)(2^{J-j}\cdot m_1). \tag{III.8}$$

The discrete wavelet transform given by (III.7) (or (III.8)) connects the wavelet transform in the continuous domain and filter banks in the discrete domain and such a connection allows the wavelet transform, initially defined in the continuous domain, to be computed with a fast algorithm based on filter banks. The connection was set up by the multiresolution analysis and it makes wavelets have had a growing impact on many fields. Our aim in this section is to derive a fast algorithm which connects continuous and digital shearlet transforms. In particular, this will lead to an explicit formula calculating the shearlet coefficients $\langle f, \psi_{j,k,m}\rangle$ in the discrete domain like the wavelet transform.

For this, we will only consider shearlets $\psi_{j,k,m}$ for the horizontal cone, i.e., belonging to $\Psi(\psi; c)$. Notice that the same procedure can be applied to compute the shearlet coefficients for the vertical cone, i.e., those belonging to $\tilde{\Psi}(\tilde{\psi}; c)$, except for switching the order of variables. We first choose a 2D scaling function and wavelet, ϕ and ψ as follows.

$$\phi(x_1, x_2) = \phi_1(x_1)\phi_1(x_2) \quad \text{and} \quad \psi(x_1, x_2) = \psi_1(x_1)\phi_1(x_2). \tag{III.9}$$

Notice that this choice of ψ satisfies (II.2) and generates a shearlet frame for $L^2(\mathbb{R}^2)$ provided that ϕ_1 and ψ_1 are sufficiently smooth and ψ_1 has enough vanishing moments. We refer to [10] for more details. Now

aiming towards a fast algorithm for computing the shearlet coefficients $\langle f, \psi_{j,k,m}\rangle$ for $j = 0, \ldots, J-1$, we first assume that

$$f(x) = \sum_{n\in\mathbb{Z}^2} f_J(n) 2^J \phi(2^J x_1 - n_1, 2^J x_2 - n_2). \tag{III.10}$$

Then observe that

$$\langle f, \psi_{j,k,m}\rangle = \langle f(S_{-k2^{-j/2}}(\cdot)), \psi_{j,0,m}(\cdot)\rangle, \tag{III.11}$$

and, WLOG we will from now on assume that $j/2$ is integer; otherwise $\lfloor j/2 \rfloor$ would need to be taken. Our observation (III.11) shows us how to compute the shearlet coefficients $\langle f, \psi_{j,k,m}\rangle$ in the digital domain: by applying the wavelet transform associated with the anisotropic sampling matrix A_{2^j} to the sheared version of the data $f(S_{2^{-j/2}k}(\cdot))$. Therefore, the main issue is how to digitize the shear operator $S_{2^{-j/2}k}$, which will provide the faithful computation of $\langle f, \psi_{j,k,m}\rangle$ in the discrete domain and our task is to define the discrete shear operator $S^d_{2^{-j/2}k} : \ell^2(\mathbb{Z}^2) \to \ell^2(\mathbb{Z}^2)$ from $S_{2^{j/2}k} : L^2(\mathbb{R}^2) \to L^2(\mathbb{R}^2)$. One problem for this is that in general, the shear matrix $S_{2^{-j/2}k}$ does not preserve the regular grid Z^2, i.e.,

$$S_{2^{-j/2}k}(\mathbb{Z}^2) \neq \mathbb{Z}^2.$$

In order to resolve this problem, we refine the regular grid $\mathbb{Z}^2$ along the horizontal axis x_1 by a factor of $2^{j/2}$. With this modification, the new grid $2^{-j/2}\mathbb{Z}\times\mathbb{Z}$ is now invariant under the shear operator $S_{2^{-j/2}k}$, since with $Q = \text{diag}(2, 1)$,

$$\begin{aligned} 2^{-j/2}\mathbb{Z}\times\mathbb{Z} &= Q^{-j/2}(\mathbb{Z}^2) = Q^{-j/2}(S_k(\mathbb{Z}^2)) \\ &= S_{2^{-j/2}k}(2^{-j/2}\mathbb{Z}\times\mathbb{Z}). \end{aligned}$$

This indicates that the shear operator $S_{2^{-j/2}k}$ is well defined on the refined grid $2^{-j/2}\mathbb{Z}\times\mathbb{Z}$, which will give us a natural discretization of $S_{2^{-j/2}k}$. From this simple observation, we now compute sampling values of $f(S_{k2^{-j/2}}\cdot)$ for sampled data $f_J \in \ell^2(\mathbb{Z}^2)$ from $f \in L^2(\mathbb{R}^2)$ as follows.

- **Step 1:** For given input data $f_J \in \ell^2(\mathbb{Z}^2)$, apply the 1D upsampling operator $\uparrow 2^{j/2}$ along the horizontal axis x_1 by a factor of $2^{j/2}$.
- **Step 2:** Apply 1D convolution to the upsampled input data f_J with 1D lowpass filter $h_{j/2}$ along the horizontal axis x_1. This gives $\tilde{f}_J$.
- **Step 3:** Resample $\tilde{f}_J$ to obtain $\tilde{f}_J(S_k(n))$ according to the shear sampling matrix S_k.
- **Step 4:** Apply 1D convolution to $\tilde{f}_J(S_k(n))$ with $\overline{h}_{j/2}$ followed by 1D downsampling by a factor of $2^{j/2}$ along the horizontal axis x_1.

In Step 1 – 2, we basically compute $\tilde{f}_J$ on the refined grid $2^{-j/2}\mathbb{Z}\times\mathbb{Z}$ which is invariant under $S_{k2^{-j/2}}$. Here, $\tilde{f}_J(n)$ are interpolated sample values from $f_J(n)$. Note that on this new grid $2^{-j/2}\mathbb{Z}\times\mathbb{Z}$, the shear operator $S_{k2^{-j/2}}$ becomes S_k with integer entries. This allows $\tilde{f}_J$ to be resampled by S_k which performs the application of $S_{k2^{-j/2}}$ to discrete data f_J in Step 3. Let $\uparrow 2^{j/2}$, $\downarrow 2^{j/2}$ and $*_1$ be 1D upsampling, downsampling and convolution operator along the horizontal axis x_1 respectively. Also, we let $\overline{h}_{j/2}(n_1) = h_{j/2}(-n_1)$. We now define the discrete shear operator which performs Step 1 – 4 as follows.

$$S^d_{2^{-j/2}k}(f_J) := \Big(((\tilde{f}_J)(S_k\cdot)) *_1 \overline{h}_{j/2}\Big)_{\downarrow 2^{j/2}} \quad \text{for} \quad f_J \in \ell^2(\mathbb{Z}^2) \tag{III.12}$$

where

$$\tilde{f}_J = ((f_J)_{\uparrow 2^{j/2}} *_1 h_{j/2}).$$

To start our analysis of the relation between the shear operator $S_{2^{-j/2}k}$ and the associated digital shear operator $S^d_{2^{-j/2}k}$, let us consider the following simple example: Set $f_c = \chi_{\{x:x_1=0\}}$. Then digitize f_c to obtain a function f_d defined on $\mathbb{Z}^2$ by setting $f_d(n) = f_c(n)$ for all $n \in \mathbb{Z}^2$. For fixed shear parameter $s \in \mathbb{R}$, apply the shear transform S_s to f_c yielding the sheared function $f_c(S_s(\cdot))$. Next, digitize also this function by considering $f_c(S_s(\cdot))|_{\mathbb{Z}^2}$. The functions f_d and $f_c(S_s(\cdot))|_{\mathbb{Z}^2}$ are illustrated in Fig. 3 for $s = -1/4$. We now focus on the problem that the integer lattice is not invariant under the shear matrix

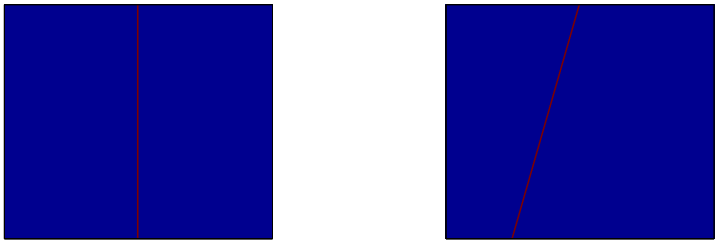

(a) (b)

Fig. 3. (a) Original image $f_d(n)$. (b) Sheared image $f_c(S_{-1/4}n)$.

$S_{1/4}$. This prevents the sampling points $S_{1/4}(n)$, $n \in \mathbb{Z}^2$ from lying on the integer grid, which causes aliasing of the digitized image $f_c(S_{-1/4}(\cdot))|_{\mathbb{Z}^2}$ as illustrated in Fig. 4(a). In order to avoid this aliasing effect, the grid needs to be refined by a factor of 4 along the horizontal axis followed by computing sample values on this refined grid.

More generally, when the shear parameter is given by $s = -2^{-j/2}k$, one can essentially avoid this directional aliasing effect by refining the regular grid $\mathbb{Z}^2$ by a factor of $2^{j/2}$ along the horizontal axis

followed by computing interpolated sample values on this refined grid. This ensures that the resulting grid contains the sampling points $((2^{-j/2}k)n_2, n_2)$ for any $n_2 \in \mathbb{Z}$ and is preserved by the shear operator $S_{-2^{-j/2}k}$. This procedure precisely coincides with the application of the digital shear operator $S^d_{2^{-j/2}k}$. Before we finish this section, we show how the discrete shear operator $S^d_{k2^{-j/2}}$ can be used to compute

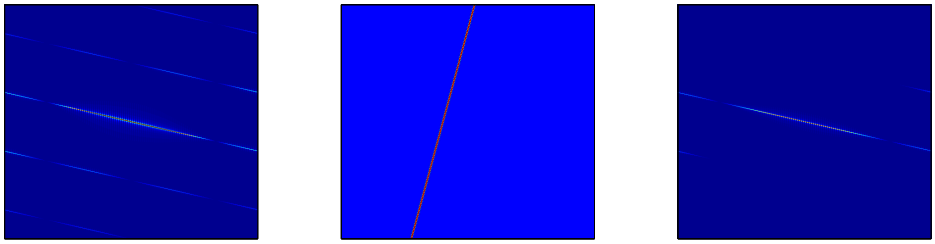

(a) (b) (c)

Fig. 4. (a) Aliased image: DFT of $f_c(S_{-1/4}(\cdot))|_{\mathbb{Z}^2}$. (b) De-aliased image: $S^d_{-1/4}(f_d)(n)$. (c) De-aliased image: DFT of $S^d_{-1/4}(f_d)(n)$.

the shearlet coefficients $\langle f, \psi_{j,k,m}\rangle$ in the discrete domain. We first define 2D separable wavelet filter W_j as follows.

$$\widehat{W_j}(\xi) = \hat{g}_{J-j}(\xi_1) \cdot \hat{h}_{J-j/2}(\xi_2).$$

Then we have the following.

Theorem III.1 ([15])**.** *Retain the notations and definitions from this subsection, and let ϕ and ψ as in* (III.9)*. Suppose that $f \in L^2(\mathbb{R}^2)$ given as in* (III.10)*. Then we obtain*

$$\langle f, \psi_{j,k,m}\rangle = \left(\overline{W}_j * \left((\tilde{f}_J(S_{-k}\cdot) * \Phi_{-k}) *_1 \overline{h}_{j/2}\right)_{\downarrow 2^{j/2}}\right)(\tilde{m}), \tag{III.13}$$

where

$$\Phi_k(n) = \langle \phi(S_k(\cdot)), \phi(\cdot - n)\rangle$$

and

$$\tilde{m} = 2^J A_{2^j}^{-1} \mathrm{diag}(c_1, c_2) m.$$

Here, $(c_1, c_2) \in \mathbb{R}^2_+$ needs to be chosen so that $2^J A_{2^j}^{-1} M_c m \in \mathbb{Z}^2$. When ϕ is an orthonormal scaling function and $k = 0$, (III.13) simply becomes the 2D discrete wavelet transform

$$\left(\overline{W}_j * f_J\right)(2^{J-j}c_1 \cdot m_1, 2^{J-j/2}c_2 \cdot m_2)$$

which is a 2D version of (III.8) associated with A_{2^j}. Also, if we remove Φ_k which behaves like the low-pass filter $h_{j/2}$, then (III.13) becomes

$$\overline{W}_j * \left(S^d_{-k2^{-j/2}}(f_J)\right)(2^{J-j}c_1 \cdot m_1, 2^{J-j/2}c_2 \cdot m_2). \tag{III.14}$$

This naturally extends the discrete wavelet transform (III.8) to compute the shearlet coefficients by adapting the discrete shear operator $S^d_{k2^{j/2}}$. Note that (III.14) computes the shearlet coefficients given in (III.11) in the digital domain by the following two basic digitization steps:

- $\psi_{j,0,m}$ is discretized by the wavelet filter W_j associated with refinement equations (III.5) and (III.6).
- The shear operator $S_{-k2^{-j/2}}$ is discretized by $S^d_{-k2^{-j/2}}$.

Of course, it is possible to compute Φ_k so that (III.13) can be explicitly implemented. However, we found that both formulations (III.13) and (III.14) perform similarly and Φ_k is not practically relevant for discrete implementation.

IV. 2D Shearlet transform with non-separable shearlet generator

Although the separable shearlet generator ψ of the form (III.9) generates a shearlet frame for $L^2(\mathbb{R}^2)$ and simplifies implementation, this choice of shearlet generator is not a good choice for directional representations. Fig. 5(a) illustrates how shearlets $\psi_{j,k,m}$ generated by separable functions cover 2D frequency domain. Because of the separability of the shearlet generator ψ, there is significant overlap between supp$(\hat{\psi}_{j,k,m})$ and supp$(\hat{\psi}_{j,k+1,m})$. In fact, this makes the ratio of frame bounds, B/A relatively large. On the other hand, as illustrated in Fig 5, wedge shaped support is well adapted for covering the frequency domain by the application of the shear and scale operators while improving directional selectivity. Motivated by this, we now consider a nonseparable shearlet generator so that its essential frequency support provides better frame bounds as well as better directional selectivity. We start by

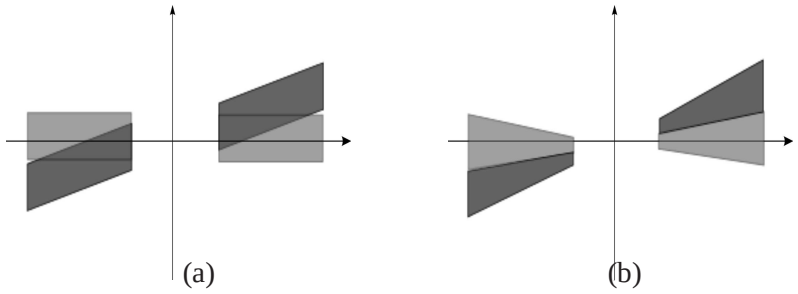

Fig. 5. Frequency covering by shearlets $\psi_{j,0,m}$ and $\psi_{j,1,m}$ (a) with separable generator (b) with non separable generator

introducing the nonseparable shearlet generator ψ^{non} as follows.

$$\hat{\psi}^{\text{non}}(\xi) = P(\xi_1/2, \xi_2)\hat{\psi}(\xi), \tag{IV.15}$$

where the trigonometric polynomial P is a 2D fan filter (c.f. [5]). Observe that ψ^{non} satisfies (II.2) and by Theorem II.3, it can be shown that the nonseparable shearlet generator ψ^{non} generate a shearlet frame for $L^2(\mathbb{R}^2)$. The proof of this immediately follows from the proof of Theorem 4.9 in [10] with a fan filter P satisfying $\inf_{\xi\in\Omega}|P(\xi)| \geq C_1$ where

$$\Omega = \{\xi \in [-1/2, 1/2]^2 : 1/4 \leq |\xi_1| \leq 1/2, |\xi_2|/|\xi_1| \leq 1\}$$

for some $C_1 > 0$. This in turn defines shearlets $\psi^{\text{non}}_{j,k,m}$ generated by ψ^{non} by setting

$$\psi^{\text{non}}_{j,k,m}(x) = 2^{\frac{3}{4}j}\psi^{\text{non}}(S_k A_{2^j} x - M_{c_j} m),$$

where M_{c_j} is a sampling matrix given by $M_{c_j} = \text{diag}(c_1^j, c_2^j)$ and c_1^j and c_2^j are sampling constants for translation.

Next, for a function f given in (III.10), we now derive a digital formulation for computing the shearlet coefficients $\langle f, \psi^{\text{non}}_{j,k,m}\rangle$ for $j = 0, \ldots, J-1$. For this, we only discuss the case of the shearlet coefficients associated with A_{2^j} and S_k; the same procedure can be applied to compute the shearlet coefficients associated with $\tilde{A}_{2^j}$ and $\tilde{S}_k$ except for switching the order of variables x_1 and x_2. First, it should be pointed out that one major drawback of the discrete algorithm (III.14) is that filtering needs to be applied to the upsampled data $\tilde{f}_J$, which requires additional computational cost by a factor of $2^{j/2}$ for each shear parameter k and scale j. To avoid this additional cost, we now consider

$$\langle f, \psi_{j,k,m}\rangle = \langle f(\cdot), \psi_{j,0,m}(S_{k/2^{j/2}}\cdot)\rangle$$

in stead of (III.11) so that the shear operator $S_{k/2^{j/2}}$ is directly applied to shearlets $\psi_{j,0,m}$. We note that

$$\langle f, \psi^{\text{non}}_{j,0,m}\rangle = (f_J * (\overline{p}_j * \overline{W}_j))(2^{J-j}c_1^j m_1, 2^{J-j/2}c_2^j m_2),$$

where $p_j(n)$ are the Fourier coefficients of a 2D fan filter given by $P(2^{J-j-1}\xi_1, 2^{J-j/2}\xi_2)$. This defines the discretization of $\psi^{\text{non}}_{j,0,m}$ by $p_j * W_j$. Using the discrete shear operator $S^d_{k2^{-j/2}}$, we now define digital shearlet filters which discretize $\psi^{\text{non}}_{j,k,m}$ originally defined in the continuum domain as follows.

$$\psi^{\text{d}}_{j,k}(n) = S^d_{k2^{-j/2}}\Big(p_j * W_j\Big)(n). \tag{IV.16}$$

The discrete nonseparable shearlet transform (DNST) associated with the non-separable shearlet generators ψ^{non} is then given by

$$DNST_{j,k}(f_J)(n) = (f_J * \overline{\psi}^{\text{d}}_{j,k})(2^{J-j}c_1^j n_1, 2^{J-j/2}c_2^j n_2) \tag{IV.17}$$

for $f_J \in \ell^2(\mathbb{Z}^2)$. Also, if we replace $p_j * W_j$ by the separable filter W_j in (IV.16), this will give digital shearlet filters associated with shearlets $\psi_{j,k,m}$ generated by the separable shearlet generator ψ. Then we call the discrete transform (IV.17) associated with the separable filters W_j the discrete separable shearlet transform (DSST). In both cases, the shearlet filters $\psi^{\mathrm{d}}_{j,k}$ can be pre-computed and (IV.17) can be then efficiently computed based on the 2D FFT without the additional computational cost especially to compute the discrete shear operator $S^d_{k2^{-j/2}}$. In Fig. 6, we compare upper and lower frame bounds for the DNST and DSST, for which we simply compute $\max_\xi \hat{\Psi}^{\mathrm{d}}(\xi)/\min_\xi \hat{\Psi}^{\mathrm{d}}(\xi)$ where $\hat{\Psi}^{\mathrm{d}}$ is defined in (IV.18). Fig. 6 shows that better frame bounds are obtained for the DNST even when it uses shearlet filters comparable with filters for the DSST with respect to the size of support. In addition to this, one major advantage of shearlets $\psi^{\mathrm{non}}_{j,k,m}$ generated by nonseparable shearlet generator is the fact that the fan filter P improves directional selectivity in the frequency domain at each scale.

Transform	A	B	B/A	Size of filter for j			
				$j=0$	$j=1$	$j=2$	$j=3$
DNST1	0.24	1.99	8.19	122×86	66×86	38×178	24×178
DNST2	0.23	2.08	9.03	22×28	14×28	10×56	8×56
DSST	0.48	7.74	16.14	106×22	50×22	22×50	8×50

Fig. 6. Numerical estimates for fame bounds A (upper) and B (lower) for the shearlet transforms with 8 8 16 16 directions. The DNST1 and DNST2 are the nonseparable shearlet transforms. For the DNST1, we use the 17×17 maximally flat 2D fan filter P and Symmlet wavelet 8-tap filter for W_j. For the DNST2, we use a 2D fan filter P generated by the $9-7$ CDF filter and Haar wavelet filter for W_j. For the DSST, we use the Symmlet wavelet 8-tap filter for W_j. We use a MATLAB routine *dfilters* from NSCT toolbox to obtain 2D fan filters we used here.

By setting $c_1^j = 2^{j-J}$ and $c_2^j = 2^{j/2-J}$, the DNST becomes a 2D convolution with shearlet filters and this gives a shift invariant linear transform. As indicated before, the digital shearlet filters $\tilde{\psi}^{\mathrm{d}}_{j,k}$ are also derived by switching the order of variables. Finally, we define separable low-pass filter by

$$\hat{\phi}^{\mathrm{d}}(\xi) = \hat{h}_J(\xi_1) \cdot \hat{h}_J(\xi_2)$$

and let

$$\hat{\Psi}^{\mathrm{d}}(\xi) = |\hat{\phi}^{\mathrm{d}}(\xi)|^2 + \sum_{j=0}^{J-1} \sum_{|k| \le 2^{\lceil j/2 \rceil}} \Big(|\hat{\psi}^{\mathrm{d}}_{j,k}(\xi)|^2 + |\hat{\tilde{\psi}}^{\mathrm{d}}_{j,k}(\xi)|^2 \Big). \tag{IV.18}$$

If $c_1^j = 2^{j-J}$ and $c_2^j = 2^{j/2-J}$, dual shearlet filters can be easily computed by,

$$\hat{\varphi}^{\mathrm{d}}(\xi) = \frac{\hat{\phi}^{\mathrm{d}}(\xi)}{\hat{\Psi}^{\mathrm{d}}(\xi)}, \ \hat{\gamma}^{\mathrm{d}}_{j,k}(\xi) = \frac{\hat{\psi}^{\mathrm{d}}_{j,k}(\xi)}{\hat{\Psi}^{\mathrm{d}}(\xi)} \quad \text{and} \quad \hat{\tilde{\gamma}}^{\mathrm{d}}_{j,k}(\xi) = \frac{\hat{\tilde{\psi}}^{\mathrm{d}}_{j,k}(\xi)}{\hat{\Psi}^{\mathrm{d}}(\xi)}. \tag{IV.19}$$

Then we obtain the reconstruction formula

$$f_J = (f_J * \overline{\phi}^{\mathrm{d}}) * \varphi^{\mathrm{d}} + \sum_{j=0}^{J-1} \sum_{|k|\le 2^{\lceil j/2\rceil}} (f_J * \overline{\psi^{\mathrm{d}}}_{j,k}) * \gamma^{\mathrm{d}}{}_{j,k} + \sum_{j=0}^{J-1} \sum_{|k|\le 2^{\lceil j/2\rceil}} (f_J * \overline{\tilde{\psi}^{\mathrm{d}}}_{j,k}) * \tilde{\gamma}^{\mathrm{d}}_{j,k}. \quad \text{(IV.20)}$$

This reconstruction formula is well defined by the frame property of shearlets generated by the nonseparable shearlet ψ^{non} (see [10]). In particular, ψ^{non} can be chosen so that

$$C_1 \le \hat{\Psi}^{\mathrm{d}}(\xi) \le C_2 \quad \text{for all } \xi \in \mathbb{R}^2$$

with some positive constants $0 < C_1 \le C_2 < \infty$.

V. 3D Shearlet transform

In this section, we derive a discrete algorithm which computes the shearlet coefficients $\langle f, \psi_{j,k,m}\rangle$, where $\psi_{j,k,m}$ are 3D shearlets defined as in Definition II.4 and assume that

$$f = \sum_{n\in\mathbb{Z}^3} f_J(n) 2^{J\cdot 3/2} \phi_1 \otimes \phi_1 \otimes \phi_1(2^J x - n).$$

Following the idea of 2D case, we choose the 3D shearlet generator ψ as follows:

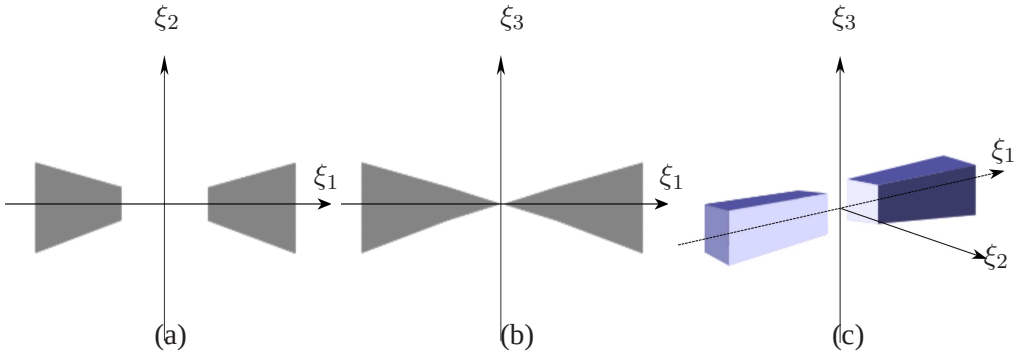

Fig. 7. 3D shearlet generator ψ in the frequency domain: (a) essential support of $P(\xi_1,\xi_2)\hat{\psi}_1(\xi_1)\hat{\phi}_1(\xi_2)$ (b) essential support of $P(\xi_1,\xi_3)\hat{\phi}_1(\xi_3)$ (c) essential support of $\hat{\psi}$

$$\hat{\psi}(\xi) = \Big(P(\xi_1/2,\xi_2)\hat{\psi}_1(\xi_1)\hat{\phi}_1(\xi_2)\Big)\cdot\Big(P(\xi_1/2,\xi_3)\hat{\phi}_1(\xi_3)\Big).$$

It should be noticed that this choice of ψ satisfies (II.4) and generates a shearlet frame for $L^2(\mathbb{R}^3)$ provided that ϕ_1 and ψ_1 are sufficiently smooth and 1D wavelet ψ_1 has enough vanishing moments. Let

$Q = \mathrm{diag}(2,1)$, then we obtain

$$\hat{\psi}_{j,k,m}(\xi) = 2^{-j}\hat{\psi}_1(2^{-j}\xi_1)\hat{\Phi}_{j,k_2}(\xi_1,\xi_2)\hat{\Phi}_{j,k_2}(\xi_1,\xi_3)E_{j,k,m}(\xi), \tag{V.21}$$

where

$$\hat{\Phi}_{j,k_1}(\xi_1,\xi_2) = (\hat{\phi}_1 \otimes P)\Big(Q^{-1}\Big(S_{-k_1}^T A_{2^j}^{-1}(\xi_1,\xi_2)^T\Big)\Big),$$
$$\hat{\Phi}_{j,k_2}(\xi_1,\xi_3) = (\hat{\phi}_1 \otimes P)\Big(Q^{-1}\Big(S_{-k_2}^T A_{2^j}^{-1}(\xi_1,\xi_3)^T\Big)\Big),$$
$$E_{j,k,m}(\xi) = \exp(-2\pi i \cdot \gamma_{j,k,m}(\xi))$$

and

$$\gamma_{j,k,m}(\xi) = (2^{-j}m_1 - k_1 2^{-j}m_2)\xi_1 + m_2 2^{-j/2}\xi_2 + m_3 2^{-j/2}\xi_3.$$

Note that Φ_{j,k_1} and Φ_{j,k_2} are functions of the form of 2D shearlets. Therefore, we discretize them in the same way as (IV.16) (without convolution with high-pass filter g_{J-j}). This gives

$$\Phi^{\mathrm{d}}_{j,k_1}(n_1,n_2) = \Big(S^d_{k_1 2^{-j/2}}(h_{J-j/2} *_1 p_j)\Big)(n_1,n_2) \tag{V.22}$$

and

$$\Phi^{\mathrm{d}}_{j,k_2}(n_1,n_3) = \Big(S^d_{k_2 2^{-j/2}}(h_{J-j/2} *_1 p_j)\Big)(n_1,n_3).$$

Here, $*_1$ is 1D convolution along the x_2 axis for the first equation and the x_3 axis for the second one. Finally, by multiresolution analysis, 1D wavelet $2^{j/2}\psi_1(2^j\cdot)$ is discretized by 1D filter g_{J-j}. Define the Fourier transform $\mathcal{F}_d : \ell^2(\mathbb{Z}^d) \to L^2([0,1]^d)$ by

$$\mathcal{F}_d(a)(\xi) = \sum_{n\in\mathbb{Z}^d} a(n)e^{2\pi i\xi\cdot n} \quad \text{for } a \in \ell^2(\mathbb{Z}^d).$$

Then, we obtain 3D digital shearlet filters which discretize $\psi_{j,k,m}$ as follows.

$$\psi^{\mathrm{d}}_{j,k} = \mathcal{F}_3^{-1}\Big(\hat{g}_{J-j}(\xi_1)\cdot\mathcal{F}_2(\Phi^{\mathrm{d}}_{j,k_1})(\xi_1,\xi_2)\mathcal{F}_2(\Phi^{\mathrm{d}}_{j,k_2})(\xi_1,\xi_3)\Big). \tag{V.23}$$

The same procedure is applied to derive 3D shearlet filters for $\tilde{\psi}_{j,k,m}$ and $\breve{\psi}_{j,k,m}$ except for switching the order of variables. Now we have the 3D discrete shearlet transform associated with the nonseparable shearlet generator ψ:

$$DNST^{3\mathrm{d}}_{j,k}(f_J)(n) = (f_J * \overline{\psi}^{\mathrm{d}}_{j,k})(\tilde{n}) \tag{V.24}$$

for $f_J \in \ell^2(\mathbb{Z}^3)$. Here,

$$\tilde{n} = (2^{J-j}c_1^j n_1, 2^{J-j/2}c_2^j n_2, 2^{J-j/2}c_3^j n_3).$$

By setting $c_1^j = 2^{j-J}$, $c_2^j = 2^{j/2-J}$ and $c_3^j = 2^{j/2-J}$, we have a shift invariant shearlet transform as in 2D case. In this case, dual shearlet filters can be explicitly computed in the same way as (IV.19). From this, a reconstruction formula is easily obtained as in (IV.20).

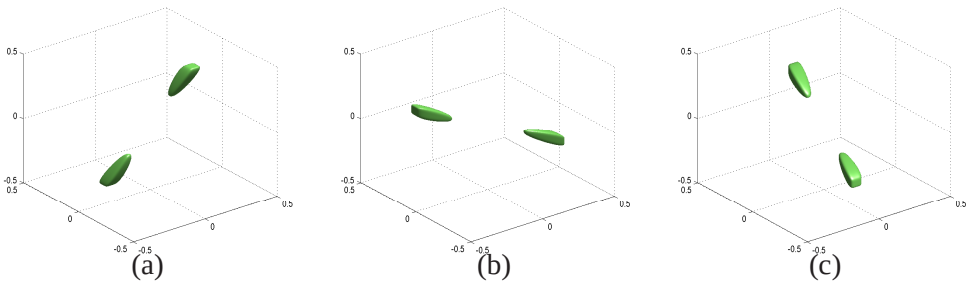

Fig. 8. 3D digital shearlets in the frequency domain: $\hat{\psi}^{\mathrm{d}}_{j,k}$

VI. Related work

We have developed a discrete framework for discretizing specific directional atoms, namely, shearlets. Shearlets $\psi_{j,k,m}$ can be viewed as the special case of parabolic molecules which are the elements of a family $(m_\lambda)_{\lambda\in\Lambda}$. Each element m_λ can be written as

$$m_\lambda(x) = 2^{3s_\lambda/4} a^{(\lambda)}(D_{2^{s_\lambda}} R_{\theta_\lambda}(x - x_\lambda))$$

such that

$$\left|\partial^\beta \hat{a}^\lambda\right| \lesssim \min\left(1, 2^{-s_\lambda} + |\xi_1| + 2^{-s_\lambda/2}|\xi_2|\right)^M (1+|\xi|)^{-N} \tag{VI.25}$$

for some positive values β, M and N. In [11], it was shown that a frame $(m_\lambda)_{\lambda\in\Lambda} \subset L^2(\mathbb{R}^2)$ satisfying (VI.25) can provide almost optimal sparse approximations for piecewise C^2 functions with a C^2 discontinuity curve and this notion of parabolic molecules can be viewed as the most general setting for directional atoms to provide sparse approximations for piecewise smooth functions in $L^2(\mathbb{R}^2)$. The above condition (VI.25) implies the Fourier transform of m_λ is essentially supported in directional wedge. This provides the directional selectivity of each element m_λ which can be used to effectively capture the edges of images. There has been extensive study in constructing and implementing directional atoms aiming at obtaining frequency localization given as in (VI.25). In particular, the various constructions of directional atoms compactly supported in the spatial domain have been introduced. We now give a short overview of some of previous works for this.

- *Contourlet transform*: Do and Vetterli first introduced compactly supported directional atoms constructed based on directional filter banks. After this, several variants have been proposed to produce directional frequency partitioning similar to those of curvelets. As the main advantage of this approach, it allows a tree-structured filter bank implementation, in which aliasing due to subsampling

is allowed to exist. Consequently, one can achieve great efficiency in terms of redundancy and good spatial localization. However, directional selectivity in this approach is artificially imposed by the special sampling rule of filter banks which often causes artifacts. In particular, it is not clear whether directional atoms constructed associated with directional filter banks satisfy the decay condition (VI.25) unless they are bandlimited functions, which means that there is no theoretical guarantee for sparse approximations for piecewise smooth images.

- *Separable shearlet transform*: The discrete shearlet transform associated with compactly supported shearlets generated by separable shearlet generator has been proposed in [15]. In this approach, the shear operator $S_{k2^{-j/2}}$ is discretized in a very crude way – it is simply given by replacing $k2^{-j/2}$ by $\lceil k2^{-j/2} \rceil$. As consequence of this crude discretization, digital shearlet filters are severely aliased in this case as illustrated in Fig. 10.

In this paper, we have introduced a new algorithmic approach for directly discretizing shearlets satisfying (VI.25) in the continuum domain. In particular, our discretization strategy based on the discrete shear operator $S^d_{k2^{-j/2}}$ provides digital shearlet filters with essentially no aliasing as illustrated in Fig. 10. Also, Fig. 9 indicates our digital shearlet filters can capture edges more effectively compared with directional transforms based on directional filter banks due to superior directional selectivity.

(a) (b) (c)

Fig. 9. Image denoising results (zoomed fragments of images): (a) Noisy image ($\sigma = 30$). (b) Denoised image with the nonsubsampled contourlet transform (NSCT). (c) Denoised image with the DNST. Both transforms have the same redundancy. Note that artifacts near the edges are reduced by the DNST due to superior directional selectivity.

VII. Applications

In this section, we will provide the numerical test results of our proposed directional transform DNST in various applications including image denoising and inpainting. For all numerical examples, we test our proposed shearlet transform given in (IV.17) for 2D examples and (V.24) for 3D examples. For our

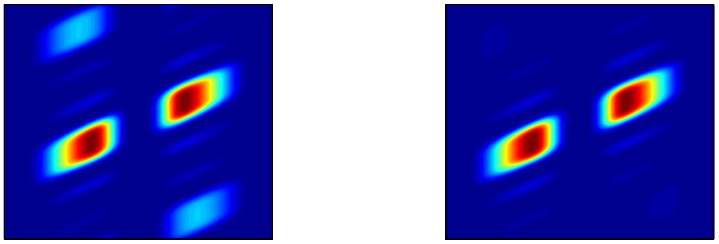

(a) (b)

Fig. 10. The magnitude of the DFT of shearlet filters generated by a separable wavelet filter: (a) Digital shearlet filter proposed in [15] (b) Digital shearlet filter with the discrete shear operator $S^{\mathrm{d}}_{k2^{-j/2}}$. Here, we use the Symmlet wavelet 8-tap filter for both cases.

tests, we use the Symmlet wavelet 8-tap filter for W_j and 17×17 maximally flat fan filter for P obtained from NSCT toolbox to compute digital shearlet filters for the DNST. For 2D case, we test two types of 4 level shearlet decompositions which are denoted by DNST1 and DNST2. For the DNST1, we apply the DNST with 8, 8, 16, 16 directions across scales. On the other hand, for the DNST2 we apply the DNST with 4, 4, 8, 8 directions across scales. For 3D case, we test two types of 3 level shearlet decompositions which are denoted by $DNST_1^{3\mathrm{d}}$ and $DNST_2^{3\mathrm{d}}$. For the $DNST_1^{3\mathrm{d}}$, we apply the 3D shearlet transform with 3, 19, 19 directions for scales $j = 0, 1, 2$, which gives redundancy factor of 42. On the other hand, for the $DNST_2^{3\mathrm{d}}$, we apply the 3D shearlet transform with 19, 67, 67 directions, which gives redundancy factor of 154. In this case, we pre-compute only 2D shearlet filters. Then all 3D shearlet filters are easily obtained as illustrated in section V. All numerical tests are performed on an Intel CPU 2.70GHz. For 2D examples, 512×512 images are used while $192 \times 192 \times 192$ images are used for 3D examples. We also refer to [12] for various numerical examples to show the effectiveness of our proposed shearlet transform in image separation.

A. 2D image denoising

First, we show comparison results in image denoising with additive Gaussian noise. For this, we compare the DNST (and the discrete separable shearlet transform DSST) with other existing directional transforms, the fast discrete curvelet transform FDCT[1][1], nonsubsampled contourlet transform NSCT [2][4] and stationary wavelet transform SWT from MATLAB wavelet toolbox. We also compare our proposed

[1]CurveLab (Version 2.1.2) is available from http://www.curvelet.org.

[2]NSCT is available from http://www.mathworks.com/matlabcentral/fileexchange/10049.

transform with other shearlet transforms, the nonsubsampled shearlet transform NSST [3][3] and discrete shearlet transform DST [4][15]. It should be pointed out that the NSST is the first published implementation of the 2D shearlet transform. In this task, an observed image g is given by

$$g = f + n,$$

where n is additive Gaussian noise and our aim is to approximate the image f from the noisy image g. For simple comparison, we apply hard threshold on the transform coefficients. For each scale j, we choose the threshold parameter T_j as

$$T_j = K_i \cdot \sigma, \tag{VII.26}$$

where σ is the standard deviation of Gaussian noise and we choose $K_j = 2.5$ for $j = 0, \ldots, 2$ and $K_j = 3.8$ for $j = 3$ for all directional transforms, the NSCT, NSST, DST, DSST, DNST1 and DNST2. And choose $K_j = 3$ for $j = 0, \ldots, 2$ and $K_j = 4$ for $j = 3$ for the SWT. For the DSST, DNST1, NSCT and NSST, 8, 8, 16, and 16 directional filters are used for scales $j = 0, 1, 2, 3$ while 4, 4, 8 and 8 directional filters are used for the DNST2. As illustrated in Fig.15 and 13, the shearlet transform outperforms other denoising schemes in terms of PSNR (peak signal to noise ratio) as well as visual quality while its running time is comparable with others.

B. Image Inpainting

Image inpainting refers to the filling-in of missing data in digital images based on the information available in the observed region. The applications of this technique include film restoration, text or scratch removal, and digital zooming. Assume that the missing pixels are indicated by an $n \times n$ diagonal maskmatrix M. The main diagonal of M encodes the pixel status, namely 1 for an existing pixel and 0 for a missing one. Also, Then we consider the following ℓ_1 minimization problem.

$$\arg \min_{Y \in \mathbb{R}^n} \|T(Y)\|_1 + \lambda \|M(X - Y)\|_2^2, \tag{VII.27}$$

where T is a linear transform $T : \mathbb{R}^n \to \mathbb{R}^m$ with $m \geq n$. Our aim here is to approximate the original image X from incomplete data $M(X)$ by minimizing the ℓ^1 norm of transform coefficients associated with T in this optimization problem (VII.27). Then restored image will be obtained by a solution to (VII.27). In this approach, it is crucial to choose the linear transform T which can sparsify the original image X

[3]NSST is available from http://www.math.uh.edu/~dlabate/software.html.

[4]DST is available from http://www.shearlab.org.

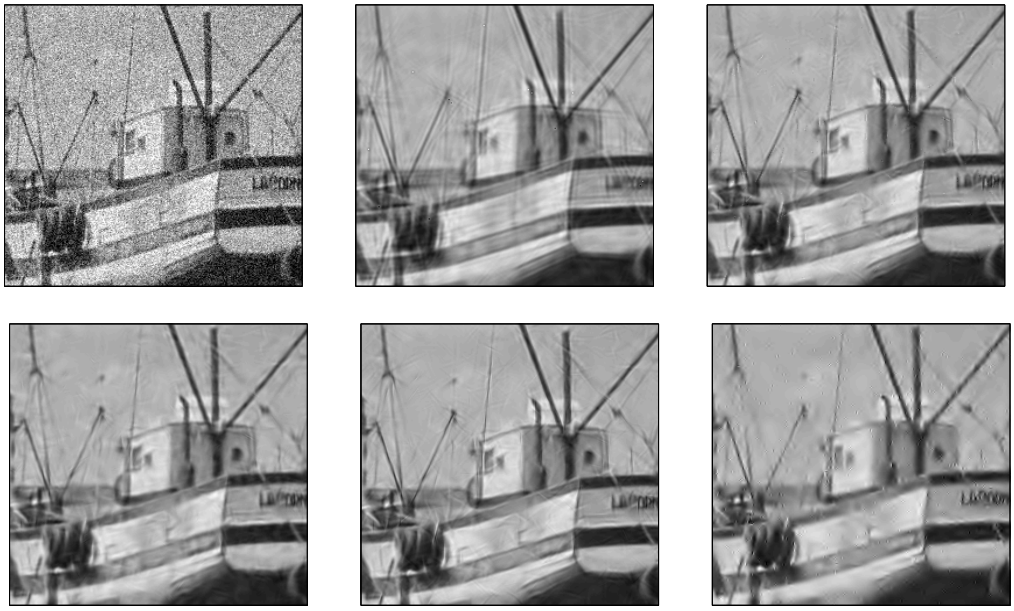

Fig. 11. Image denoising results with various transforms. (a) From Left to Right (Top): Noisy Boat image ($\sigma = 30$), FDCT (27.72dB), NSST (28.65dB). (b) From Left to Right (Bottom): NSCT (28.61dB), DNST1 (29.01dB), SWT (27.27dB).

Transform	NSCT	SWT	FDCT	NSST	DNST1	DNST2	DST
Running time	266.24 sec	0.57 sec	0.48 sec	5.98 sec	1.48 sec	0.78 sec	1.57 sec
Redundancy	53	13	5.64	49	49	25	20

Fig. 12. Comparison of running times for denoising schemes with various transforms for 512×512 image: running times for computing shealret filters for the DNST1 and DNST2 are 1.25sec and 0.50sec respectively.

in the transform domain in order to successfully restore X from $M(X)$. This sparsity model (VII.27) for image inpainting was introduced and several numerical experiments showed the effectiveness of this approach in [6]. We apply the same iterative threshold scheme described in [6] to approximately solve (VII.27). We now present numerical experiments with various test images to compare the performance of inpainting schemes using the FDCT(MCALab)[5], DNST1, DSST and DST. For our tests, we simply apply

[5]MCALab (Version 120) is available from http://www.greyc.ensicaen.fr/~jfadili/demos/WaveRestore/downloads/mcalab/Home.html.

	Lena				Barbara				Peppers			
σ	10	20	30	40	10	20	30	40	10	20	30	40
NSCT	35.43	32.35	30.51	29.17	33.07	29.16	27.01	25.54	33.99	31.57	29.97	28.73
SWT	34.52	31.05	29.00	27.57	31.96	27.57	25.36	24.05	33.48	30.67	28.69	27.32
FDCT	34.00	31.31	29.54	28.24	29.14	25.62	24.58	24.02	32.60	29.93	28.45	27.43
NSST	35.50	32.57	30.71	29.31	32.97	29.45	27.31	25.84	34.12	31.86	30.23	28.98
DNST1	**35.90**	**32.75**	**30.84**	**29.41**	33.64	**30.03**	**27.84**	**26.33**	**34.44**	**32.17**	**30.59**	**29.31**
DNST2	35.79	32.38	30.25	28.64	33.38	29.45	27.08	25.41	34.40	31.99	30.26	28.87
DSST	35.79	32.38	30.25	28.64	**33.65**	29.70	27.27	25.54	34.38	31.84	30.04	28.56
DST	35.74	32.27	30.28	28.81	33.71	29.78	27.56	26.07	34.21	31.58	29.87	28.59

	Man				F16				Boat			
σ	10	20	30	40	10	20	30	40	10	20	30	40
NSCT	32.46	29.61	28.07	27.02	34.59	31.49	29.58	28.17	33.63	30.37	28.61	27.39
SWT	31.80	28.51	26.81	25.61	33.85	30.47	28.27	26.79	32.91	29.18	27.27	25.93
FDCT	31.06	28.63	27.19	26.09	33.37	30.05	28.06	26.83	31.56	29.18	27.72	26.56
NSST	32.62	29.73	28.09	26.94	34.68	31.57	29.50	28.19	33.77	30.47	28.65	27.30
DNST1	33.05	**30.04**	**28.34**	**27.13**	34.99	**31.88**	**29.89**	**28.60**	34.23	**30.87**	**29.01**	**27.63**
DNST2	33.10	29.96	28.20	26.93	35.03	31.90	29.82	28.48	34.09	30.63	28.71	27.27
DSST	**33.29**	30.00	28.11	26.73	**35.11**	31.92	29.75	28.35	**34.29**	30.69	28.64	27.11
DST	32.96	29.67	27.93	26.70	34.96	30.57	29.43	28.08	34.24	30.56	28.59	27.17

Fig. 13. Comparison results (PSNR values) for various denoising schemes.

	Lena			Barbara			Peppers		
	PSNR	Iter	Time	PSNR	Iter	Time	PSNR	Iter	Time
FDCT	31.23dB	300	590.26sec	27.59dB	300	590.26sec	30.61dB	300	590.26
DNST1	**32.54dB**	126	202.92sec	**28.12dB**	126	202.92sec	**31.89dB**	126	202.92sec
DSST	31.27dB	126	202.92sec	27.11dB	126	202.92sec	30.34dB	126	202.92sec
DST	31.77dB	135	225.23sec	27.96dB	135	225.23sec	31.15dB	135	225.23sec

	Man			F16			Boat		
	PSNR	Iter	Time	PSNR	Iter	Time	PSNR	Iter	Time
FDCT	27.45dB	300	590.26sec	29.26dB	300	590.26sec	28.75dB	300	590.26
DNST1	**28.69dB**	126	202.92sec	**29.89dB**	126	202.92sec	**29.37dB**	126	202.92sec
DSST	28.07dB	126	202.92sec	28.27dB	126	202.92sec	27.61dB	126	202.92sec
DST	28.34dB	135	225.23sec	29.74dB	135	225.23sec	28.82dB	135	225.23sec

Fig. 14. Inpainting results: PSNR, the number of iterations and running time.

1

the DNST1(and DSST) with 8, 8, 16, 16 directions in (VII.27), where T is the DNST1 (and DSST). Our numerical tests show that DNST1 outperforms other transforms. In particular, the edges of inpainted images are well captured due to the superior directional selectivity of DNST1.

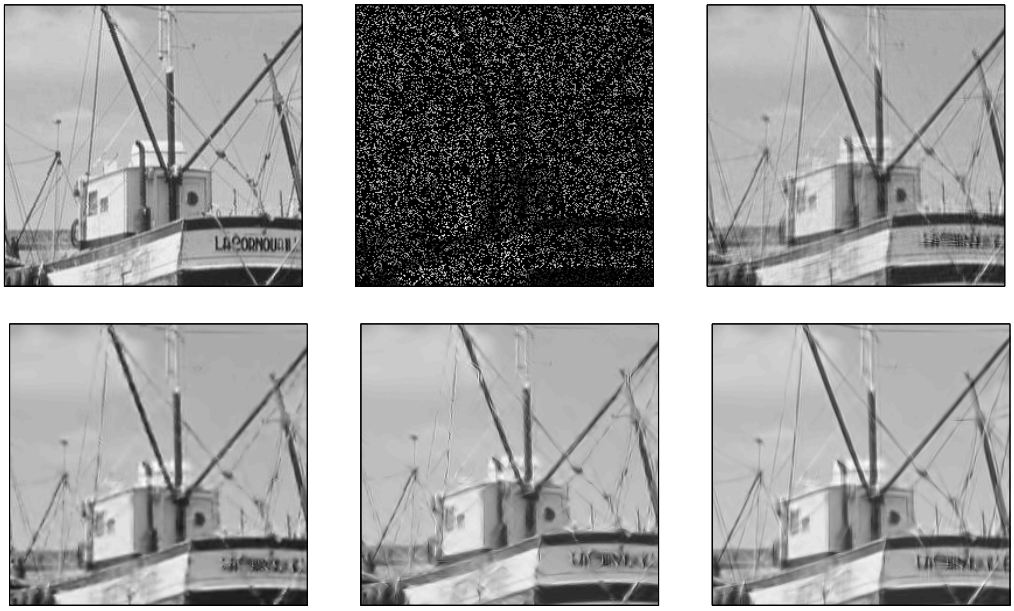

Fig. 15. Image inpainting results with various transform. (a) From Left to Right (Top): Original image , 80% missing pixels, FDCT (28.75dB). (b) From Left to Right (Bottom): DST (28.82dB), DSST (27.61dB), DNST1 (29.37dB).

C. Video Denoising

We finally present the numerical test results of the 3D shearlet transform in 3D video denoising tasks. As in 2D denoising tests, we apply various linear transforms followed by hard threshold to remove additive Gaussian noise – here, basic settings for the tests are the same as 2D image denoising tests. For the 3D discrete shearlet decomposition, we apply a 3-level decomposition. We have tested two different types of the shearlet transforms, the $DNST_1^{3\text{d}}$ and $DNST_2^{3\text{d}}$ – they differ only by the number of directions across scales as we explained in the beginning of this section. We compared the performance of our shearlet based denoising scheme with other state-of-the-art directional transforms: the surfacelet transform (denoted by Surf) [6] [16] and 3D band-limited shearlet transform (denoted by Band-Shear) [17]. It should be noted that Band-Shear is the first 3D shearlet transform. The numerical results of Band-Shear are taken from [17]. We use two test video sequences Mobile and Coastguard ($192 \times 192 \times 192$) and choose $K_j = 4$ for the finest scale and $K_j = 3$ for the rest of scales in (VII.26).

[6]SurfBox is available from http://www.mathworks.com/matlabcentral/fileexchange/14485.

	Surf	Band-Shear	$DNST_1^{3d}$	$DNST_2^{3d}$
Redundancy	6.4	208	42	154
Running time	30.90sec	263sec	45.12sec	165.97sec

Fig. 16. Redundancy and running time for each of 3D transforms.

	Mobile					Coastguard				
Noise (σ)	10	20	30	40	50	10	20	30	40	50
Surf	33.05	30.25	28.56	27.34	**26.40**	31.02	28.42	27.05	26.08	25.33
Band-Shear	NA	NA	28.68	27.15	25.97	NA	NA	27.36	26.10	25.12
$DNST_1^{3d}$	34.87	30.93	28.60	26.96	25.69	32.59	29.04	27.16	25.85	24.85
$DNST_2^{3d}$	**35.42**	**31.55**	**29.30**	**27.66**	26.38	**33.58**	**29.92**	**27.93**	**26.55**	**25.45**

Fig. 17. Video denoising results.

VIII. Conclusion

In this paper, we have developed a new discrete shearlet transform associated with compactly supported shearlets generated by a nonseparable generator which provides good localization in space domain as well as improved directional selectivity. It is based on the discrete shear transform $S^d_{k2^{-j/2}}$ which faithfully digitizes the shear operator $S_{k2^{-j/2}}$ in the continuum domain. In fact, combining multiresolution analysis in theory of wavelets, this framework allows the shearlet coefficients $\langle f, \psi_{j,k,m}\rangle$ to be explicitly computed in the discrete domain. We also showed the various applications of our directional transform in image processing. In numerical tests, our proposed transform compares favorably with other existing directional transforms. In particular, the superior directional selectivity and localization property of compactly supported shearlets reduces artifacts to enhance visual quality of restored image. One major drawback of our discrete framework is that our transform is not fully structured unlike the discrete wavelet transform or other directional transforms based on filter banks. Therefore, our future study will be focused on structured directional transforms based on our proposed discrete framework.

References

[1] E. J. Cand‘es, L. Demanet, D. L. Donoho and L. Ying, *Fast discrete curvelet transforms*, SIAM Multiscale Model. Simul. **5** , 861–899, (2006).

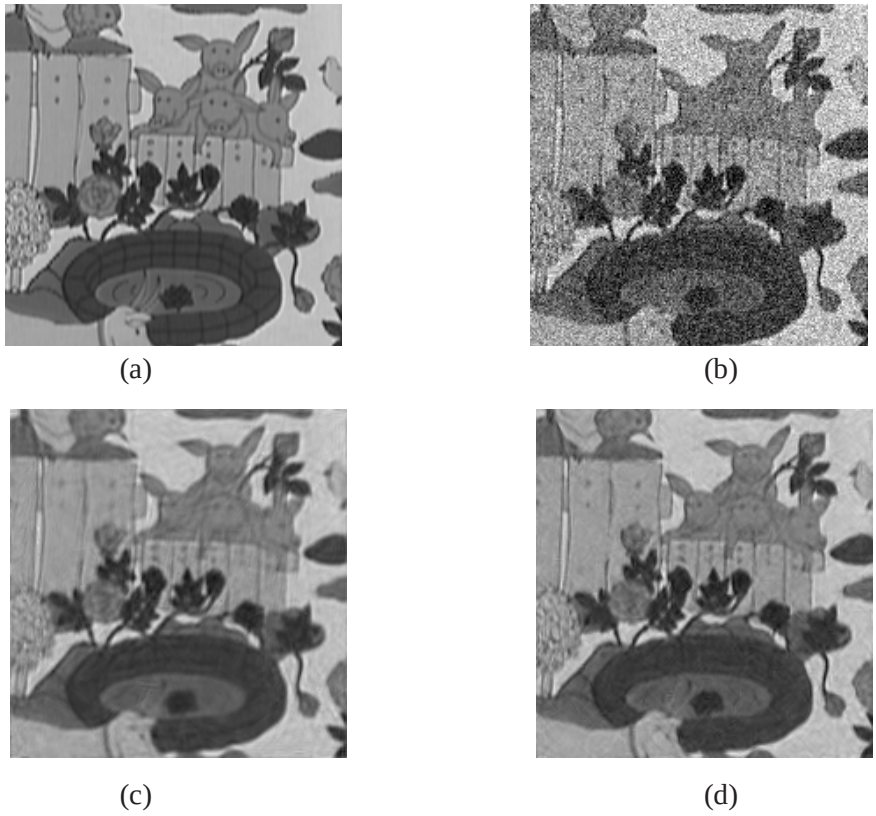

Fig. 18. Video Denoising of Mobile Video Sequence. The figure compares the denoising performance of the denoising algorithm based on the 3D shearlet transform, $DNST_2^{3d}$, on a representative frame of the video sequence Mobile against video denoising routine based on the surfacelet transform denoted as Surf. (a) Original frame (b) Noisy frame (18.62dB) and denoised frame using (c) Surf (28.56dB) (d) $DNST_2^{3d}$ (29.30dB)

[2] E. J. Cand'es and D. L. Donoho, *New tight frames of curvelets and optimal representations of objects with C^2 singularities*, Comm. Pure Appl. Math., **57**, 219–266, (2004).

[3] G. Easley, D. Labate and W. Lim, "Sparse directional image representations using the discrete shearlet transform", Appl. Comput. Harmon. Anal. **29**, (2010).

[4] A. L. Cunha, J. Zhou, and M. N. Do, *The nonsubsampled contourlet transform: Theory, design, and applications*, IEEE Trans. Image Proc., **15**, 3089–3101, (2006).

[5] M. N. Do and M. Vetterli, *The contourlet transform: an efficient directional multiresolution image representation*, IEEE Trans. Image Proc. **14**, 2091–2106, (2005).

[6] M. Elad, J.-L Starck, D. Donoho and P. Querre, *Simultaneous Cartoon and Texture Image Inpainting using Morphological Component Analysis (MCA)*, Appl. Comput. Harmon. A., **19**, 340–358, (2005).

[7] K. Guo, G. Kutyniok, and D. Labate, *Sparse multidimensional representations using anisotropic dilation and shear operators*, Wavelets and Splines (Athens, GA, 2005), Nashboro Press, Nashville, TN, 189–201, (2006).

[8] G. Kutyniok, J. Lemvig, and W.-Q Lim. *Optimally Sparse Approximations of 3D Functions by Compactly Supported Shearlet Frames*, SIAM J. Math. Anal., to appear.

[9] G. Kutyniok and W.-Q Lim, *Compactly Supported Shearlets are Optimally Sparse*, J. Approx. Theory, **163**, 1564–1589, (2011).

[10] P. Kittipoom, G. Kutyniok, and W.-Q Lim, *Construction of Compactly Supported Shearlet Frames*, Constr. Approx., **35**, 21–72, (2012).

[11] P. Grohs and G. Kutyniok. *Parabolic Molecules*, Prepint (2012).

[12] G. Kutyniok and W.-Q Lim. *Image Separation using Wavelets and Shearlets*, Curves and Surfaces (Avignon, France, 2010), Lecture Notes in Computer Science **6920**, Springer, (2012).

[13] G. Kutyniok, M. Shahram, and X. Zhuang. *ShearLab: A Rational Design of a Digital Parabolic Scaling Algorithm*, Submitted.

[14] D. Labate, W.-Q Lim, G. Kutyniok, and G. Weiss. *Sparse multidimensional representation using shearlets*, Wavelets XI (San Diego, CA, 2005), 254–262, SPIE Proc. **5914**, SPIE, Bellingham, WA, (2005).

[15] W.-Q Lim, *The discrete shearlet transform: A new directional transform and compactly supported shearlet frames*, IEEE Trans. Image Proc., **19**, 1166–1180, (2010).

[16] Y. M. Lu and M. N. Do, *Multidimensional directional filter banks and surfacelets*, IEEE Trans. Image Proc., **16**, 918–931, (2007).

[17] P. S. Negi and D. Labate, *3D discrete shearlet transform and video processing*, IEEE Trans. Image Process., **21**, 2944–2954, (2012).